Solution Structure of 2-(Pyrido[1,2-*e*]purin-4-yl)amino-ethanol Intercalated in the DNA Duplex d(CGATCG)$_2$[†]

Adrien Favier,[‡] Martin Blackledge,[‡] Jean-Pierre Simorre,[‡] Serge Crouzy,[§] Vincent Dabouis,[∥] Alain Gueiffier,[⊥] Dominique Marion,*[,‡] and Jean-Claude Debouzy[∥]

Institut de Biologie Structurale, 41 rue Jules Horowitz, 38027 Grenoble Cedex 1, France, CRSSA, Unité de Biophysique, 24 avenue des maquis du Grésivaudan, 38702 La Tronche Cedex, France, Centre d'Etudes Nucléaires de Grenoble, BP 85X, avenue des Martyrs, 38000 Grenoble, France, and Laboratoire de Chimie Thérapeutique, Faculté de Pharmacie de Tours, 31 avenue Monge, 37200 Tours, France

Received October 27, 2000; Revised Manuscript Received March 9, 2001

ABSTRACT: The solution structure of the complex formed between d(CGATCG)$_2$ and 2-(pyrido[1,2-*e*]-purin-4-yl)amino-ethanol, a new antitumor drug under design, has been resolved using NMR spectroscopy and restrained molecular dynamic simulations. The drug molecule intercalates between each of the CpG dinucleotide steps with its side chain lying in the minor groove. Analysis of NMR data establishes a weak stacking interaction between the intercalated ligand and the DNA bases; however, the drug/DNA affinity is enhanced by a hydrogen bond between the hydroxyl group of the end of the intercalant side chain and the amide group of guanine G6. Unrestrained molecular dynamic simulations performed in a water box confirm the stability of the intercalation model. The structure of the intercalated complex enables insight into the structure−activity relationship, allowing rationalization of the design of new antineoplasic agents.

In aggressive tumors, the nuclear DNA of malignant cells often replicates more quickly than the nuclear DNA of surrounding healthy tissues (*1*). Interference in DNA replication of malignant cells inhibits tumor expansion, and reduces tumor mass if unsuccessful replication induces tumor cell death (*2*). A substantial fraction of effective anticancer drugs bind nuclear DNA, either covalently or noncovalently, and interfere with replication (*3*). The most prominent examples in general clinical use are the anthracycline antibiotics adriamycin and daunomycin, the anthracenedione mitoxandrone, and the antileukemic 9-anilinoacridineamsacrine (*4*). However, both the development of acquired resistance and the severity of toxicity associated with antineoplasic agents have necessitated the continuing development of new drugs.

Mutagen derivative compounds can be considered as interesting starting molecules due to their high affinity for DNA, although their chemical characteristics have to be modified to reduce mutagenic properties while retaining high intercalant activity. Classical studies have shown that mutagens can be formed in mixtures of amino acids or proteins which are treated by high temperature or by pyrolysis (*5*−*8*). Potent mutagens have thus been isolated from pyrolysates of ornithine, lysine, D,L-phenylalanine, tryptophan, and glutamic acid. In particular, isosteric 2-aminofluorene compounds, including amino-γ-carboline derivatives (Trp-P-1 and Trp-P-2) and aminodipyridoimidazole derivatives (Glu-P-1 and Glu-P-2), have been identified as being highly mutagenic (*9*−*11*).

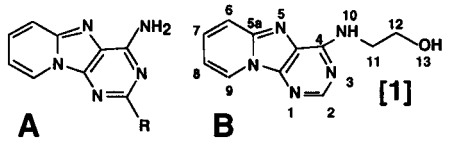

FIGURE 1: (A) Structure of the pyridopurine skeleton. (B) Structure of the pyridopurine exhibiting the best DNA intercalation and transmembrane crossing properties, showing the atom numbering scheme.

In a series of studies on novel compounds having the imidazopyridine skeleton, the intercalation characteristics of azaindolizine derivatives of Glu-P, i.e., imidazopyridine and pyridopurine derivatives (Figure 1A), were initially investigated (*12*). A preliminary screening of potential intercalation properties of these molecules was performed using natural salmon sperm DNA and the synthetic oligonucleotides d(CGATCG)$_2$ and d(ACATGT)$_2$ as targets. From the previously described criteria (*13*), based on chemical shift variations and line-broadening of imino proton resonances, two pyridopurines were identified as potential intercalants, although even these rough tests already indicated that the intercalation properties of the pyridopurines were found to be relatively weak and nonspecific.

Subsequent efforts to achieve better antitumor activity focused on pyridopurine derivatives. Thus, Debouzy et al. (*14*) showed that pyridopurine derivatives exhibited both lower mutagenic properties and higher levels of DNA

[†] This work has been supported by the Centre National de la Recherche Scientifique, Commisariat à l'Energie Atomique. A.F. was a recipient of a MESR fellowship.

* To whom correspondence should be addressed. E-Mail: dominique.marion@ibs.fr. Telephone: (33) 4 38 78 36 98. Fax: (33) 4 38 78 54 94.

[‡] Institut de Biologie Structurale.

[§] Centre d'Etudes Nucléaires de Grenoble.

[∥] CRSSA, Unité de Biophysique.

[⊥] Laboratoire de Chimie Thérapeutique, Faculté de Pharmacie de Tours.

10.1021/bi0024963 CCC: $20.00
Published on Web 07/06/2001

fixation. The aromatic part of these pyridopurine derivatives was found to be responsible for specific intercalation into the DNA helix between intact Watson−Crick C-G base pairs (*15*). The goal of the chemical structure modifications was to enhance both the intercalation properties and the biocompatibility of the drug, i.e., its ability to cross the cellular membrane (*12*). The control of the hydrophobic/hydrophilic balance was considered as a key point for the synthesis and was achieved by attaching different side chains to the pyridopurine core, the amphiphilic properties of the side chain affecting the overall solubility of the molecule.

The best overall performance, as measured by transmembrane transport and drug−DNA intercalation, was achieved using 2-(pyrido[1,2-*e*]purin-4-yl)amino-ethanol, or **[1]** (*16*), whose side chain is composed of two methyl groups joining the pyridopurine 4-positioned NH group with the terminal hydroxyl group (Figure 1B). Biological assays showed that this molecule was the most active in vitro against tumor stems MCF7 and HL60 of the synthesized pyridopurine derivatives; however, the activity of **[1]** remained too weak to begin clinical tests. At this stage of the development, a rational strategy to design a new antitumor compound from **[1]** with an enhanced activity requires the understanding of the mechanisms of interaction of **[1]** with its DNA target using the information contained in the structure of the complex.

NMR spectroscopy is an ideal tool for studying the structural and dynamic bases of intermolecular complexes. In recent years, this technique has thus provided an understanding of the intercalation properties of a number of DNA-binding drugs. In this study, we use 1D and 2D homonuclear NMR spectroscopy combined with simulated annealing/rMD[1] to characterize the interaction of **[1]** with $d(CGATCG)_2$. The stability of the complex was then investigated by unrestrained MD.

MATERIALS AND METHODS

Sample Preparation. The self-complementary hexamer $d(CGATCG)_2$ (nomenclature: 1C-2G-3A-4T-5C-6G), purchased from the Pasteur Institute (Paris), was used without further purification and dissolved in a buffer containing 160 mM KCl, 0.15 mM EDTA, 20 mM sodium phosphate at pH 7 in either pure D_2O or (for the observation of exchangeable protons) D_2O/H_2O, 10%/90%. In the former case, the solution was lyophilized and resuspended in 99.98% D_2O and degassed. The dried drug was then added to the DNA sample in order to saturate the solution, and thereby maximize the population of drug in the intercalation sites.

NMR Assignment of the DNA−Drug Complex. Standard phase-sensitive 2D NMR experiments, recorded at 400 MHz, were used to assign the nonexchangeable proton chemical shifts of the complex, including 2D-DQF-COSY (*17, 18*), 2D-TOCSY (*19*−*21*), and 2D-NOESY (*22, 23*).The mixing time was set at 250 ms for NOESY and at 80 ms for TOCSY.

The exchangeable proton assignment was completed using a WATERGATE NOESY (*24*) experiment performed at 800 MHz (mixing time: 100 ms).

^{31}P NMR spectra were acquired as for the proton spectra using standard acquisition and composite pulse proton decoupling. All experiments were recorded at 280 K.

NOE-Based Distance Restraints. NOESY spectra (with mixing times of 50 and 100 ms) were acquired in D_2O and H_2O at 800 MHz ^1H frequency at a temperature of 280 K. In D_2O, the residual water resonance was irradiated during the relaxation delay and the mixing period, and in H_2O a WATERGATE filter was added. A total of 96 scans per FID were acquired with a 1.7 s intertransient delay. The time domain data (400 × 2048 complex points) were multiplied by a squared cosine function and zero-filled to yield final spectra with 1024 × 2048 data points. Convolution difference was used during processing only for the spectra dedicated to the exchangeable proton observation. The strong diagonal signals of the drug protons produced significant baseline distortions compared to the drug−DNA cross-peak intensities. To overcome this difficulty, a cubic-spline baseline correction was applied specifically along the rows and columns corresponding to the drug proton resonances.

Peak volumes from NOESY experiments were measured using Felix (10/97, MSI) and calibrated using the fixed distances H5−H6 of cytosines C_1 and C_5 (2.45 Å). Distances were estimated from NOEs recorded with mixing times of 50 and 100 ms. As the global correlation time of the intercalant was unknown, we classified the drug/DNA distances as medium (4 Å) or weak (6 Å), and the intramolecular NOEs observed in the drug were not used for the structure calculation of the complex. Unresolved protons were replaced by pseudo-atoms, and an appropriate correction was applied to the measured distance (*25*).

Chemical shift variation versus temperature was monitored using a NOESY experiment recorded at 298 K.

^{31}P NMR. Structural information concerning the DNA backbone was derived from measurement of the three-bond ($^1H_{3'}-^{31}P$) *J*-coupling related to backbone dihedral angle ϵ of the DNA by the semiempirical Karplus type equation: $^3J(H_{3'}-P) = 15.3\cos^2(\epsilon + 120°) - 6.2\cos(\epsilon + 120°) + 1.5$ Hz (*26, 27*). Two CT ^1H-^1H COSY experiments in the presence or absence of a 180° ^{31}P pulse during the CT period (*28*) were performed at 400 MHz and 298 K on the sample dissolved in D_2O. The coupling constant $J(H_{3'}-P)$ is deduced from the ratio of the ^1H-^1H peak intensity measured in the two ^1H-^1H CT COSY (*29*) by the equation:

$$\Delta = \frac{I_{\text{attenuated}}}{I_{\text{reference}}} = \cos(2\pi^3 J_{H_{3'}-P} T)$$

$2T$ being the time-constant length.

The two experiments were performed in an interleaved manner with otherwise identical parameters. The errors were derived from the uncertainty induced by the presence of noise, the rms value of which is measured in resonance-free regions of both spectra. A total of 1024 and 200 complex points were acquired in the direct and indirect dimensions respectively, and data were apodized by a squared cosine function and zero-filled in the two dimensions to yield final spectra with 512 × 1024 data points. The attenuation factor of the signal with and without ^{31}P decoupling was derived

[1] Abbreviations: FID, free induction decay; DQF-COSY, double quantum filtered correlated spectroscopy; TOCSY, total correlated spectroscopy; NOE, nuclear Overhauser effect; NOESY, nuclear Overhauser effect spectroscopy; HMQC, heteronuclear multiple quantum spectroscopy; rms, root-mean-square; RHF, restricted Hartree Fock; MD, molecular dynamic; rMD, restrained molecular dynamic.

from H2′−H3′ cross-peak volume integration in both experiments. A 50 ms constant-time period was used to obtain the best compromise between the loss of signal due to the H3′ transverse relaxation and the $^3J_{H3'-P}$ coupling transfer efficiency.

Structure Calculations. Structure calculations were performed using the program DISCOVER interfaced with INSIGHT II for visualization and analytical purposes (Molecular Simulations Inc.). The AMBER4 force field was used for simulated annealing calculations. A skewed biharmonic energy function (*30*) was used for constraints application. An upper bound uncertainty of 20% was applied to D_2O-derived restraints, and an error of 50% for distances estimated from NOESY performed in H_2O. The lower distance limit was effectively equivalent to the sum of the van der Waals radii of the two protons. A total of 428 distances were used in the structure determination procedure.

To achieve a broad sampling of the conformational space, the simulated annealing protocol was started from different sets of randomized Cartesian coordinates. During this calculation, nonbonded interactions were replaced by a simple quartic repulsive term (*31*−*34*). A sigmoid switching function was initiated at 4 Å, and all nonbound contacts were ignored at interatomic distances greater than 6 Å. The atomic radius was taken to be 0.825 of the van der Waals radius defined in the AMBER force field. For all calculations, a leapfrog algorithm using steps of 1 fs was employed, and the list of the neighboring atoms was updated every 20 fs. The exploratory period was calculated at a nominal temperature of 1000 K. Scaling of various energy terms was performed as in previously published protocols (*35*). The experimental data were introduced such that k_{NOE} values were scaled from 0.02 to 20 or from 0.1 to 100 kcal mol^{-1} Å^{-2}, for the DNA/DNA and drug/DNA distances, respectively, after the scaling period of 30 ps was complete. Once this first step of simulated annealing was complete, the temperature was dropped linearly to 600 K in 1 ps, and the weight of the experimental distances was reduced to 0.1 kcal mol^{-1} Å^{-2}.

This exploratory calculation was followed by a refinement stage where the quartic nonbond interaction is replaced by a standard Lennard−Jones potential and a distance-dependent dielectric constant to mimic the effect of the solvent (*36*, *37*). After 1 ps equilibration at 600 K, the temperature is linearly increased back to 1000 K in 4.5 ps. For 10 ps, k_{NOE} is gradually raised to the maximum values of 20 or 100 kcal mol^{-1} Å^{-2} for the DNA/DNA and drug/DNA distances, respectively. The complex is then allowed to evolve during another 10 ps of dynamics simulation with all experimental restraints set to the maximum value. The complex is cooled over a period of 5 ps until the target temperature of 100 K is reached, at which point a further 1 ps of dynamics is performed. All structures obtained after this restrained molecular dynamics protocol were minimized using the conjugate gradients algorithm.

Molecular Simulation. To test the stability of the complex after removing all the restraints, we ran short MD simulations in a realistic aqueous environment, following the protocol already described in a previous report (*15*).

The charges and geometry of **[1]** were optimized at the ab initio RHF/6-31G* level of theory using GAMESS (*38*). With the energy minimizations being done around the local minimum closest to the input structure, dihedral angles in the most mobile part of the molecule, N3−C4−NH−C11, C4−NH−C11−C12, and NH−C11−C12−O13, were varied independently in steps of 60°, and a geometry optimization calculation was run for each conformation. The structure of **[1]** with lowest ab initio energy will be called "global" minimum energy structure in this work.

Partial charges were deduced from the calculation of the electrostatic potential following the CHELPG (*CHarges from ELectrostatic Potential Grid*) algorithm with additional constraints to satisfy the total charge and dipole of the molecule.

All parameters for DNA and ions were taken from the CHARMM22 force field (*39*), and parameters for **[1]** (other than charges) come from the extended CHARMM/Quanta force field (*40*). The structure of the DNA−drug complex shown in Figure 5 was used as initial coordinates for the present modeling study. Ten potassium counterions were initially placed at the O−P−O bisector of each phosphate linking group, 3 Å away from the phosphorus atoms. The system DNA + **[1]** + 10 potassium ions was immersed into a 40 Å side box of equilibrated water molecules. Waters with oxygen atoms closer than 2.5 Å from any nonwater heavy atom (non-H) were discarded, yielding a total system of 1961 water molecules and 6327 atoms. Periodic boundary conditions for nonbonded interactions were applied in all three dimensions for a cubic box of 40 Å side, with 12 Å cutoff. Particle mesh Ewald was used to compute electrostatic interactions. Energy minimizations and molecular dynamic (MD) simulations were run with CHARMM (*36*). Shake (*41*) was applied to all bonds involving hydrogen atoms.

Restraints were initially introduced between potassium ions and nearby phosphorus atoms to prevent escape of the ions, and non-hydrogen atoms of DNA were harmonically restrained to their original position during stage (1) below. Restraints between K^+ and P were then removed, and three short MD simulations were run with different distance restraints:

(1) 10 000 steps MD with 24 restraints listed in Table 4 between drug and DNA + H-bond distance restraints between H21 and O13 (Figure 6A) or between N3 and H13 (Figure 6B), with force constant 10 kcal mol^{-1} Å^{-2}.

(2) 10 000 steps MD with H-bond distance restraints only, with force constant 10 kcal mol^{-1} Å^{-2}.

(3) 50 000 steps MD with no restraints.

These Langevin dynamics MD simulations were run at $T = 300$ K with a friction of 10 ps^{-1} applied on every nonhydrogen atom and a time step of 2 fs.

Unrestrained MD simulations were run on a pentium PC cluster at the CEA in Grenoble.

RESULTS

The 2:1 Binding Stoichiometry for the ***[1]***−*d(CGATCG)$_2$ Complex.* As described previously, intercalating drugs, groove binders, and nonspecific outside binders can be easily identified by monitoring the chemical shift and line width variation of imino protons. Successive spectra of d(CGATCG)$_2$ were then recorded in the presence of increasing amounts of **[1]** as shown from bottom to top in Figure 2A. All imino resonances continuously shift toward higher fields upon drug addition, while no new peak is detected even at

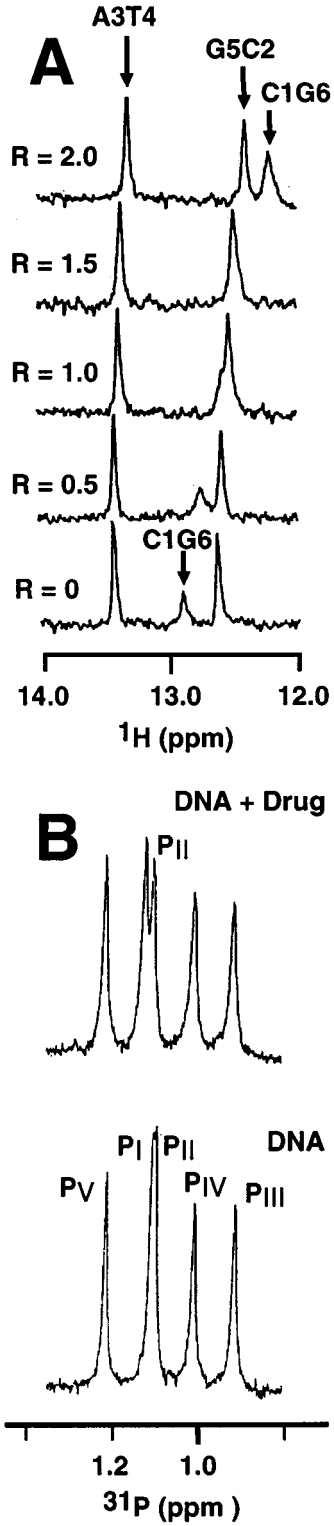

FIGURE 2: Titration of d(CGATCG)$_2$ by **[1]**. (A) ^{1}H NMR chemical shift variations of the imino protons implicated in Watson−Crick base-pairing starting from 4 mM DNA, *R* being the drug:DNA ratio. The spectra were recorded at 277 K on a 400 MHz spectrometer. (B) ^{31}P NMR spectra of pure d(CGATCG)$_2$ (283 K, 4 mM, bottom trace) and in the presence of equimolar pyridopurine derivatives (top trace). Phosphorus nomenclature: 5′-C_{P_I}-$G_{P_{II}}$-$A_{P_{III}}$-$T_{P_{IV}}$-C_{P_V}-G-3′. Assignment of the ^{31}P nuclei of d(CGATCG)$_2$ was performed on the free form. Both titration experiments were performed using increasing drug to DNA ratios, allowing the peaks of each nucleus to be followed during the titration.

275 K, indicating a fast exchange between free and bound species (*42*). As described elsewhere, such an evolution is generally considered as evidence for intercalation (*43*). Imino protons of the GC base pairs are significantly more shifted than those of the AT pairs [0.5 ppm (C1G6), 0.3 ppm (C5G2) against 0.15 ppm (AT) for **[1]**/d(CGATCG)$_2$ = 2, M/M], indicating a preferential GC intercalation. Following similar experiments performed under constant total concentration ([drug] + [dCGATCG] = 4 mM), Job plots (*44*) (not shown) were derived from the chemical shift variations of GC pairs. A plot of the chemical shift variations, weighted by the concentration as a function of the molar fraction (*F*), shows a maximum when the stoichiometry is reached. In this case, $F = 0.5$, which indicates that two molecules of **[1]** can intercalate the duplex d(CGATCG)$_2$.

^{1}H Resonance Assignment. (A) Nonexchangeable Protons. The assignment was accomplished following the analysis of NOESY (mixing time 250 ms), COSY-DQF, and TOCSY spectra recorded on the D_2O sample. The palindromic base sequence of d(CGATCG)$_2$ is responsible for a high symmetry in the NMR spectra, which remains unbroken by the presence of the intercalative drug. The DNA spin systems remain degenerate such that each NOE cross-peak corresponds to the same interproton distance in each DNA strand. The neighboring nucleotides were identified using the deoxyribose H1′ (5.4−6 ppm) to base H6−H8 (6.5−8.5 ppm) correlation and cytosine H5−H6 COSY correlations as reference points (*25*).

Indeed, the palindromic symmetry of the system implies that two intercalative sites are available for the drug, confirming the 2:1 binding stoichiometry measurement for the pyridopurine derivative−d(CGATCG)$_2$ complex.

(B) Exchangeable Protons. The observation of NOEs between the imino protons of guanine bases and the amino protons of the hydrogen-bonded partner cytosine bases in the NOESY (H_2O) spectrum establishes Watson−Crick pairing at all dG·dC base pairs in the duplex. Similarly, the observation of NOEs between imino protons of thymine and the H2 and amino protons of adenine residues establishes Watson−Crick pairing at all dA·dT base pairs in the duplex. Distance restraints between atoms involved in the Watson−Crick hydrogen bonding pairs were imposed in the structure calculations based on this experimental evidence.

^{31}P NMR Spectroscopy. ^{31}P NMR spectroscopy has been extensively used to probe DNA intercalation since this mode of binding generally leads to downfield shifts of the ^{31}P NMR signals around the intercalating site (*45*). The spectrum of native d(CGATCG)$_2$ (283 K) presented on the bottom trace of Figure 2B shows five resonances that were assigned using experimental data, references from the literature (*46*), and HMQC control experiments. The spectrum recorded in the presence of **[1]** shows that most of the ^{31}P resonances are not affected by the presence of the drug. However, the PI line (see nomenclature in the legend of Figure 2B) was clearly downfield-shifted.

Analysis of Phosphodiester Backbone. The phosphodiester backbone structure of nucleic acids, containing very few protons, cannot be precisely defined using NOE distance restraints exclusively. To provide better resolution, we measured the vicinal ^{1}H3′−^{31}P *J*-coupling constants (see Table 1) which characterize the ϵ (C4′−C3′−O3′−P) angle. The observed couplings range from 2 to 6 Hz, consistent with torsion angle values of 140−200°. Because of the multivalued character of the Karplus curve, the additional

Table 1: $^3J(H_{3'}-P)$ Scalar Coupling Constants Measured along the DNA Backbone

nucleotide	J(H3′−P) (Hz)[a]
G2	5.41 ± 0.56
A3	3.48 ± 0.75
T4	<2.05
C5	<1.67
G6	6.25 ± 0.51

[a] $^3J(H_{3'}-P)$ coupling constants are related to the backbone dihedral angle ϵ (C4′−C3′−O3′−P) by a semiempirical Karplus-type relation.

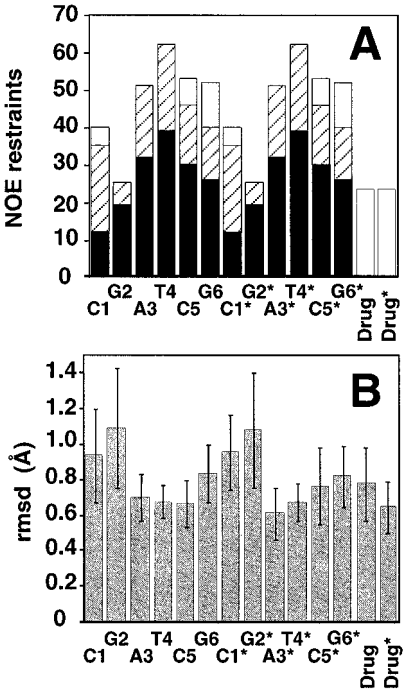

FIGURE 3: (A) Distribution of NOE restraints applied in the structural refinement. Due to the palindromic symmetry of the complex, each NOE cross-peak corresponds to two distances (one per DNA strand). Of the 202 intranucleotide distances derived from the NOESY experiments and incorporated in the restrained MD, 37 were found not structurally significant. Hatched bars, intranucleotide NOEs; solid bars, internucleotide NOEs; open bars, drug−DNA NOEs. (B) Rms deviation of the atoms of each nucleotide of the ensemble from the mean values. It is worth noting that the palindromic symmetry was not used to constrain the DNA during the restrained MD calculations, explaining the slight rms deviation differences between the two DNA strands.

range of 270° < ϵ < 350° is consistent with the measured $^3J_{H3'-P}$, but such values are rare in deoxyribonucleotides. Moreover, strong correlations observed in a short mixing time NOESY (50 ms) between H6/H8 base protons and H2′/H2″ sugar protons of the same nucleotide indicate near-C2′-endo conformations for the sugars, and thus B-type duplex (*25*) for which $^3J_{H3'-P}$ torsion angles are approximately 155°.

Experimental Restraints. A set of 282 intra-DNA distances were derived from nonexchangeable ^{1}H NOE volumes and 64 intra-DNA distances from exchangeable ^{1}H NOEs. The intra-DNA distances consisted of 202 intranucleotide restraints and 144 internucleotide restraints. The distribution of these restraints with respect to base is displayed in Figure 3A. The localization of the intercalation sites in the vicinity of C1-G2, and the evidence that the central nucleic acids adopt a canonical B-DNA form, allowed us to consider all DNA−DNA NOESY peak volumes as emanating from

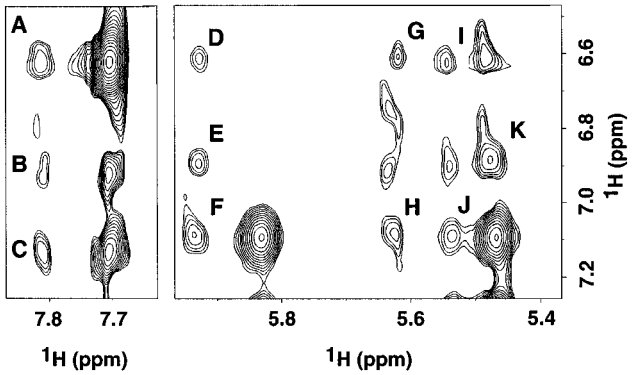

FIGURE 4: Expanded NOESY (100 ms at 800 MHz) contour plots of the drug−d(CGATCG)$_2$ complex in D_2O buffer at 280 K showing NOEs between the protons of the drug and the protons of the hexamer. The labels of the drug−DNA cross-peaks (A−K) are given Table 4.

Table 2: Energetic and Experimental Statistics of the **[1]**−DNA Complex

Energetic Statistics[a]	
bond	4.97 ± 0.64
angle	56.3 ± 3.6
dihedral	199.4 ± 4.1
out-of-plane	1.09 ± 0.07
H-bond	−3.27 ± 0.23
VDW	−144 ± 4
elec. static	−602 ± 3
total	−487 ± 6
Experimental Statistics	
no. of distance violations >0.05 Å	2.0
violation energy[a]	5.70 ± 1.73
maximum violation	0.19 Å

[a] Values in kcal mol^{-1}.

symmetric inter- or intra-strand interactions. All drug−DNA cross-peaks were treated as originating from two symmetric interactions. The restraints are evenly distributed along the length of the oligodeoxynucleotide, except for nucleotide G2. The small number of NOE restraints defining this nucleotide (33 compared with 66 for T4) is due to overlapping resonances preventing accurate measurement of cross-peak volumes. A set of 10 $^3J_{H3'-P}$ torsion angle restraints were introduced into the structure calculations. The restraints also included 32 empirical distances imposed on the atoms involved in the Watson−Crick pairs. A total of 24 drug−DNA NOE cross-peaks whose pattern is shown in Figure 4 could be extracted from the NOESY spectrum in D_2O buffer. It is worth noting that an important intra-drug NOE was observed implicating the H12 proton of the external CH_2 of the side chain and the H2 proton of its aromatic moiety.

Structure Analysis. We have chosen to use structure calculations starting from randomized coordinates rather than from any kind of intercalation model which could introduce artifacts in the structure determination of the complex. Over 100 structure calculations were performed using the protocol described under Materials and Methods; 22 were selected on the basis of the low experimental and physical energy. These emergent structures define a single ensemble in which the rms deviation from the mean of all atoms is 0.8 Å. Table 2 summarizes the energetic and experimental statistics of the molecular modeling procedure. No important energetically unfavorable nonbounded contacts were produced from these distances. Only two distance violations greater than

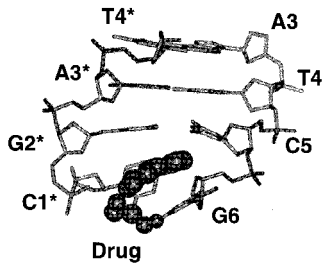

FIGURE 5: Binding mode of the 2:1 complex of **[1]** with d(C-GATCG)$_2$ represented by the closest structure of the NMR ensemble from the mean structure (PDB code 1I5V). View looking from the intercalation site into the minor groove of the oligomer. The bases labeled with an asterisk belong to one strand of DNA; the bases labeled without an asterisk belong to the complementary strand.

0.05 Å were observed on average, leading to relatively small energy values (6 kcal/mol) and demonstrating the coherence of the NOE restraints data set with the final structure.

Sugar and Backbone Conformation. Excluding the 5′-terminal nucleotide C1, the majority of the deoxyribose rings adopt the "south" conformation in the range of 120−160°. The sugar puckering observed in our NMR structure ensemble is supported by the qualitative analysis of the *J*-couplings found in the DQF-COSY spectrum which are characteristic of the C2′-endo conformation. The glycosidic angles, χ, correspond to the anti conformation typically found in the B-DNA (*25*). The values of the torsion angles of the backbone of the structure ensemble are also distributed close to the values found in the B form for most of the nucleotides. However, significant torsion angle disorder is observed for G2 whose α, ζ , β, and γ angles are distributed in four different regions, one of which represents the canonical form of B-DNA. The convergence of the structure ensemble can be better characterized by the rms deviation (from the mean) for the atoms of each nucleotide depicted in Figure 3B. Except for the C1, G2 nucleotides, the whole complex, whose rms deviations vary between 0.6 and 0.8 Å, is well-defined. The larger rms deviation displayed by G2 is almost certainly due to the small number of NOE restraints defining this nucleotide (33 compared with 66 for T4) due to overlapping resonances preventing accurate measurement of cross-peak volumes.

*Intercalated Conformation of **[1]** and DNA Interaction.* The aromatic moiety of **[1]** is intercalated between the external GC base pairs (Figure 5), with the side chain of **[1]** lying in the minor groove of the hexamer. The terminal hydroxyl group of the side chain appears to form a H-bond interaction with guanine G6 of the DNA. In most of the structures (38 out of 44), a hydrogen bond is possible between the extremity of the drug side chain (oxygen O13) and guanine G6 (amide proton H21 and nitrogen N2) (Figure 6A). The other hydrogen bond found in the second intercalation model involves the hydrogen H13, the oxygen O13 of the extremity of the drug side chain, and the nitrogen N3 of the guanine G6 (Figure 6B). To test the stability of the drug−DNA complex, two unrestrained molecular dynamic calculations were conducted starting from the two H-bond schemes observed in the NMR structure ensemble.

Unrestrained Molecular Dynamics in a Water Box. Ab initio molecular simulation performed on the drug alone in a vacuum showed that the structure of **[1]** with minimum energy is planar up to carbon C11 of the tail. Characteristic

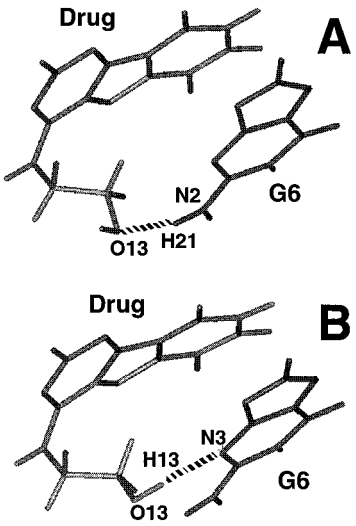

FIGURE 6: Drug−base (G6) stacking interaction in the intercalation site. On the top is displayed the H-bond observed in 38 out of 44 intercalation structures. On the bottom is displayed the H-bond observed in 6 out of 44 intercalation structures.

Table 3: Characteristic Angles and Dihedrals of the Structure of **[1]**

atoms	angle (deg)[a] (a)	(b)
C4−NH−C11	125.9	127.6
NH−C11−C12	115.2	114.1
C11−C12−O13	112.8	112.8
N3−C4−NH−C11	−7.6	174.7
C4−NH−C11−C12	71.3	92.1
NH −C11−C12−O13	−87.3	−60.6

[a] Angles and dihedrals of the lowest energy conformation of **[1]** are listed in column (a). Angles and dihedrals of the second lowest energy conformation of **[1]** are listed in column (b).

angles and dihedrals are listed in Table 3, column (a). Noticeably, in this conformation the molecule establishes a hydrogen bond (distance 2.0 Å) between H13, the hydrogen bonded to the oxygen, and N3. Moreover, the mirror image of the molecule with respect to the plane of the rings, with identical bond angles and dihedral angles C4−NH−C11−C12 = −71.3° and NH−C11−C12−O13 = 87.3°, has the same minimum energy as the one presented. A geometry optimization starting from coordinates of **[1]** derived from the refinement (Figure 5) leads to a structure with energy 1.6 kcal/mol higher than the "global" minimum just described and angles listed in Table 3, column (b). This structure is stabilized by a H-bond between H13 and N5. Both ab initio optimized structures are shown in Figure 7.

Unrestrained MD calculations were conducted on the **[1]**−d(CGATCG)$_2$ complex in a water box starting from the two intercalation models corresponding to the two types of drug/DNA H-bonds obtained after the restrained MD calculation stage. Of the two interaction models studied, only one, model A in Figure 6, yielded a stable insertion of **[1]** inside DNA with more than half of the initial NOE restraints satisfied after 100 ps free MD. The corresponding average structure obtained after stage 3 is shown in Figure 8. The color range from blue to red represents the average rms deviations from 0.5 to 2.5 Å of the atoms from the average structure determined with NMR restraints (water molecules and ions have been omitted for the sake of clarity). Clearly, the drug and CG external DNA base pairs present the largest

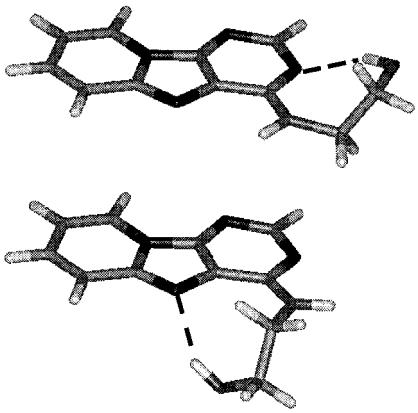

FIGURE 7: Ab initio optimized structures of **[1]** in a vacuum. The lowest energy structure is displayed on the top of the figure. The second lowest energy structure is displayed on the bottom of the figure. Intramolecular H-bonds are displayed with dashed lines.

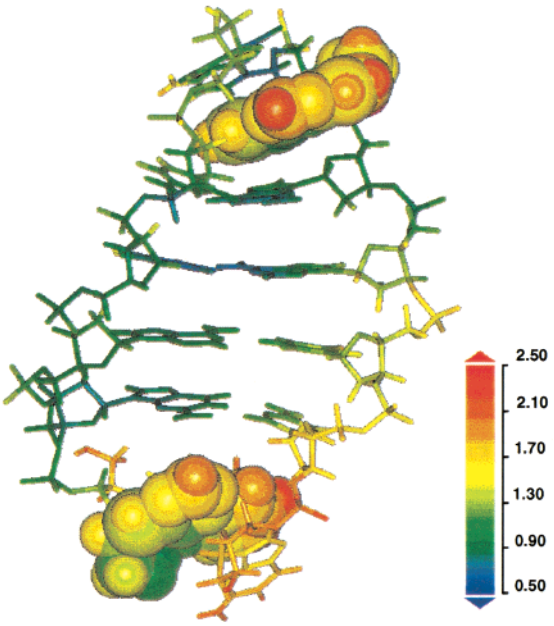

FIGURE 8: Binding mode of the 2:1 complex of **[1]** with d(CGATCG)$_2$; mean structure from the 100 ps unrestrained MD in a water box. The color range from blue to red represents the root-mean-square deviations from 0.5 to 2.5 Å of the atoms from the average structure determined with NMR restraints (water molecules and ions have been deleted for clarity).

fluctuations consistent with the NMR results. The average distance between H21 and O13 is 3.6 Å with a rms deviation of 1.2 Å; its value is less than 3 Å 45% of the time in one site and 30% of the time in the other insertion site, which means that this H-bond seen during the refinement (Figure 6A), although weak, is stable on a 100 ps time scale. Starting from the hydrogen bonds corresponding to scheme B in Figure 6 yields structures where the drug is still inserted between CG base pairs but has lost the N3−H13 H-bond (average distance of 6.2 Å) and where most of the NOEs in Table 4 are not satisfied, on average.

Inspection of the MD trajectory, during which the drug remains inserted for 100 ps, leads to the following observations: Watson−Crick base−base H-bond distances are conserved during the simulation with an average value around 2 Å; average Watson−Crick base−base distance C1′−C1′ and base−base angle N1−C1′−C1′ for pyrimidines

Table 4: Intermolecular NOEs Observed between [**1**] and DNA Protons

drug protons	DNA[a]
H2	G6(H1′); G6(H2′)
H6	C1(H2″)
H7	G6(H1′)(D); G6(H8)(**A**); C1(H5)(**G**); C5(H1′)(**I**)
H8	C5(H6); G6(H8)(**C**); G6(H1′)(**F**); C1(H5)(**H**); C5(H1′)(**J**)
H9	G6(H1′)(**E**); C5(H1′)(**L**); G6(H2′); C5(H2″); C5(H6)(**K**)
H11	C1(H1′)
H12	C1(H5); C1(H1′); G6(H8); G6(H1′); G6(H2′); G6(H2″)

[a] Some of the DNA protons are followed by a boldface letter (A−K) labeling the intermolecular NOE cross-peaks plotted in Figure 4.

or N9−C1′−C1′ for purines are 10.7 Å and 56.4° with rms deviations of 0.5 Å and 8°, respectively, in agreement with standard values for B-DNA [10.85 Å and 51.5° (*36*)]. Values of ϵ (C4′−C3′−O3′−P) lie between −132 and −155° for internal bases, close to the range of NMR allowed values. They drop to −112, −119, −147, and −129° for external bases which are much more mobile.

DISCUSSION

Structure Calculation. Both d(CGATCG)$_2$ proton and phosphorus chemical shift variations suggest an intercalation of the aromatic fragment of the molecule at the level of the C1G2 bases. Due to the severe lack of long-range distance constraints defining the tertiary structure of DNA, many structure determination protocols of the drug−DNA complex start from structures obtained by sandwiching the drug (or the adduct) between two fragments of B or A canonical DNA. In our case, an unambiguous starting model could not be constructed from the measured drug−duplex NOE restraints using this approach. The use of randomized initial coordinates to determine the structure of the complex allows a more extensive sampling of conformational space and effectively removes the possibility of artifacts linked to the starting intercalation model. Using such a calculation protocol, we observed conformational convergence for structures in agreement with the measured NOE restraints, permitting unambiguous identification of the intercalation characteristics of **[1]** with d(CGATCG)$_2$ (Figure 5).

Drug/DNA Stacking Interactions and Intermolecular Hydrogen Bonding. The characteristic chemical shift changes due to the alterations in base stacking that accompany intercalation have allowed ^{1}H chemical shift perturbation to be widely adopted as a qualitative analysis of DNA binding modes of both intercalators and groove binders. In this study, relatively large upfield shifts are observed for the protons of the pyridopurine ring system in the range −0.3 to −0.4 ppm during the titration of d(CGATCG)$_2$ by the drug up to the stoichiometric ratio, indicative of stacking interactions with the DNA base pair. In contrast, resonances from the side chain of the drug undergo more modest changes in shift, consistent with its position in the minor groove. A view normal to the helix axis and looking into the minor groove of d(CGATCG)$_2$ of a representative structure of the NMR ensemble is presented in Figure 9A, and a view looking down the helix axis of the oligomer at the intercalation site is shown in Figure 9B. It can be seen that the pyridopurine derivative rings are not exactly perpendicular to the helix

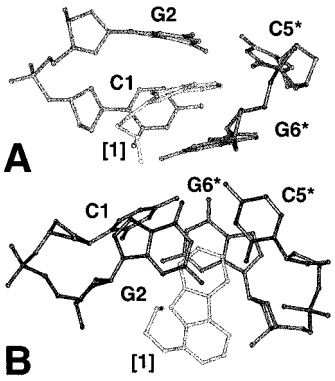

FIGURE 9: Top view looking into the minor groove and normal to the helix axis of $d(CGATCG)_2$ at the intercalation site. Bottom view looking down the helix axis of $d(CGATCG)_2$ of a representative structure of the NMR structure ensemble. The bases labeled with an asterisk belong to one strand of DNA; the bases labeled without an asterisk belong to the complementary strand.

axis, with the drug stacking between the guanine G2 of one strand of the duplex and the guanine G6 of the other strand. The drug is not completely buried in the helical stack, but the stacking interaction seems to concern mainly the external ring of the drug comprising protons H6, H7, H8, and H9. The preferential stacking of the pyridopurine derivative on base G6 is stabilized by two alternative hydrogen bonding interactions (Figure 6). From the unrestrained MD study, the hydrogen bond involving H13 and O13 of the extremity of the drug side chain and nitrogen N3 of guanine G6 appears far less stable than the hydrogen bond concerning oxygen O13 of the drug side chain and amide proton H2 and nitrogen N2 of guanine G6. The ability of the aromatic cycle of the drug to form a H-bond with its H13 hydrogen was also confirmed by the ab initio study of the drug in a vacuum, where both the lowest and second lowest energy structures (Figure 7) show this same possibility of H-bond formation. The ability of the latter (with an energy only 1.6 kcal/mol higher than the "global" minimum energy structure) to form a hydrogen bond with the duplex may be sufficient to make it the most stable in the presence of solvent and DNA.

It is generally admitted that four-ring heterocyclic molecules are good basic structures to obtain intercalating properties in DNA (*47*). Although the aromatic moiety of **[1]** is composed of three rings, ab initio calculations performed on **[1]** in a vacuum and in the absence of DNA clearly showed that the side chain substitution on the third ring leads to stable "pseudo-fourth ring" formation by folding of the acyl chain. Experimentally, the connectivity observed between the H2 proton of the third cycle and the H12 proton of the terminal methylene group reveals that the side chain is folded, rather than free as generally found for acyl chains. The resulting "pseudo" ring should enhance the stacking and intercalation interactions and may result in a supplementary activity enhancement.

On the other hand, the base C1 is not involved in the intercalation process and does not stack with its upper base G2. The tilt of cytosine C1 is supported by 1D ^{31}P NMR spectra of $d(CGATCG)_2$ recorded in the presence and absence of the drug. The phosphorus located between cytosine C1 and G2 is the only phosphorus of the duplex whose chemical shift changes (Figure 2B). This chemical shift variation reflects a different electronic environment of the cytosine C1 caused by the presence of the drug and/or a small backbone conformation rearrangement between C1 and G2. However, if the intercalation site was in the middle of the oligomer sequence, the tilt of the cytosine C1 should be stabilized by the upper base stacking. It would therefore be interesting to derive further evidence for this hypothesis by studying the interaction of the pyridopurine derivative with an oligomer whose GC intercalation is in the center of the sequence.

*Comparison of Binding Models of **[1]** and 9-Amino-DACA with DNA.* A large number of mono-intercalants share common structural features. In many cases, they are composed of a polycyclic aromatic core exhibiting stacking interactions with the acid nucleic bases. The drug activity is often enhanced by additional chemical compounds attached to the intercalated aromatic moiety, such as sugars, side chains, or aromatic cycles. These compounds may promote trans-membrane transport and facilitate interaction with the minor or major groove of the DNA via hydrogen bonds, van der Waals interactions, or electrostatic interactions. Among these mono-intercalant compounds, the 9-amino-DACA has the most homology with **[1]** in terms of chemical structure and DNA interaction mechanisms. 9-Amino-DACA is a derivative of the 9-aminoacridine-4-carboxamide class of compounds which are potent cytotoxins and also intercalate into GC-rich sequences of DNA. The structure of 9-amino-DACA complexed with the DNA hexanucleotide $d(CGTACG)_2$ has recently been resolved by X-ray crystallography (*48*). **[1]** and 9-amino-DACA both have an aromatic core of three cycles and a side chain composed of one amino group and two methyl groups. However, the side chain of **[1]** ends with a hydroxyl group whereas 9-amino-DACA ends with a 2-dimethylamine. Although the side chain of **[1]** lies in the minor groove of the hexamer whereas the side chain of 9-amino-DACA lies in the major groove, the conformations of the two intercalation processes are close: in both cases, the drugs intercalate between two GC base pairs, and the high affinity of these two molecules with their DNA target is enhanced by strong intermolecular H-bond interactions. The hydroxyl group of the side chain of **[1]** exhibits a hydrogen bond with the amide group of G2 whereas the carboxamide NH group of 9-amino-DACA hydrogen bonds to a structurally important water molecule which in turn hydrogen bonds to the phosphate group of guanine G2.

*The Antitumor Activity of **[1]** Is Provided by the Multiconformational Properties of Its Side Chain.* A previous study of drug−membrane interaction strongly suggested an unfolded conformation of the side chain of **[1]** in membrane models (*16*, *49*), possibly to improve trans-membrane transport. In contrast, the two ab initio lowest energy structures of **[1]** demonstrate the ability of the drug to fold its side chain into a fourth "pseudo-cycle", probably allowing a better intercalation property into the helical stack of the nucleic acids. Moreover, the NMR solution structure determination of the **[1]**−$d(CGATCG)_2$ complex (Figure 5) shows a more packed conformation of the drug inside the DNA, the side chain of the **[1]** extremity being H-bonded to G6 of the oligomer.

It may be important to reinforce electrostatic interactions between the end of the side chain and the heterocycles of the drug to strengthen the stability of the fourth pseudocycle. One possibility would be the addition of negative charge to

the aliphatic chain. In view of the observed intermolecular H-bond between the terminal methylene group of **[1]** and intracyclic NH_2 (G3), it appears that the negative charge conferred at this point by a carboxyl group could provide a significant stability of the drug inside DNA, even if no direct chemical bond occurs (*50*). The effect of such a replacement on the electrostatic interactions with DNA would, of course, need to be carefully monitored.

CONCLUSION

A pyridopurine derivative **[1]** has been studied with a view to enhancing its antitumor activity. In this article, we have determined the solution structure of the complex formed between **[1]** and the oligonucleotide model d(CGATCG)$_2$ by NMR spectroscopy and rMD simulations. The structure ensemble verifying the NMR restraints confirms the intercalation specificity of the pyridopurine core for DNA CG base pairs as described previously (*15*). The structure highlights the multiconformational property of the side chain of **[1]**, allowing transmembrane transport in an unfolded conformation (*49*) and enhancing the drug/DNA affinity in a more packed conformation (Figure 9). The stacking of **[1]** with d(CGATCG)$_2$ is stabilized by a hydrogen bond implicating oxygen O13 of the extremity of the drug side chain and amide proton H2 and nitrogen proton N2 of guanine G6.

When allowed to evolve freely in a realistic aqueous environment, the most populated conformational models present in the NMR ensemble were stable, and satisfied over half of the distance restraints seen by NMR spectroscopy, after 100 ps. The fact that we never observed a complete escape of the drug from its site after total removal of the distance restraints during our unrestrained MD simulations supports the idea that the drug/DNA interactions are sufficient to stabilize the complex.

It is worth noting that the oligonucleotide d(CGATCG)$_2$ used here is rather short and that the intercalation sites are located at the extremity of the molecule. However, this hexanucleotide is considered as a classical target for testing intercalators (*51*−*54*), due to its variety of potential sites of intercalation; however, longer oligonucleotides, with several different intercalation sites, would seriously complicate NMR investigation due to conformational exchange or low symmetry. Our simple model does not permit the evaluation of the long-range propagation of the deformation induced by the intercalation. Similar tests were performed on natural DNA from salmon sperm, and similar shifts of CG imino resonances were found in the presence of drug. It would therefore be interesting to study the next generation of pyridopurine derivatives complexed with a DNA duplex whose GC intercalative site is located at its center. Most of the work done on antitumor drug/DNA structure concerned molecules already used for cancer therapy with very high intercalation property with deoxyribonucleic acids. Here, we show that NMR spectroscopy is a good tool to follow at a molecular level the interaction of a drug under development and its target.

ACKNOWLEDGMENT

We thank M.S.I. (San Diego, CA) for the continuing collaboration.

SUPPORTING INFORMATION AVAILABLE

Expanded NOESY contour plots of the drug−d(CGATCG)$_2$ complex in D_2O establishing sequential distance connectivities, expanded NOESY contour plots of the drug−d(CGATCG)$_2$ complex in H_2O buffer, backbone and heavy atoms of the 21 NMR structure of the **[1]**−d(CGATCG)$_2$ complex, plot of the backbone torsion angles (α vs ζ, β vs γ, and δ vs ϵ), and plot of the glycosidic χ angle versus the pseudo-angle *P* for each nucleotide (4 pages). This material is available free of charge via the Internet at http://pubs.acs.org.

REFERENCES

1. Bentley, N. J., and Carr, A. M. (1997) *Biol. Chem. 378*, 1267−1274.
2. McIntosh, E. M., and Haynes, R. H. (1997) *Acta Biochim. Pol. 44*, 159−171.
3. Pratt, W. B., Ruddon, R. W., Ensminger, W. D., and Maybaum, J. (1994) in *The anticancer drugs*, Oxford Press, New York.
4. Malonne, H., and Atassi, G. (1997) *Anti-Cancer Drugs 8*, 811−822.
5. Hashimoto, Y., Takeda, K., Shudo, K., Okamoto, T., Sugimura, T., and Kosuge, T. (1978) *Chem.-Biol. Interact. 23*, 137−140.
6. Kosuge, T., Tsuji, K., Wakabayashi, K., Okamoto, T., Shudo, K., Iitaka, Y., Itai, A., and Seino, Y.-T. (1978) *Chem. Pharm. Bull. Tokyo 26*, 611−619.
7. Matsukura, T., Kawashi, N., Morino, K., Ohgaki, H., Sugimura, T., and Takayama, S. (1981) *Science 213*, 346−347.
8. Yamaizumui, Z., Shiomi, T., Kasai, H., Nishimura, S., Takayashi, Y., Nagao, M., and Sugimura, T. (1980) *Cancer Lett. 9*, 75−83.
9. Tsuda, M., Takayashi, Y., Nagao, M., Hirayama, T., and Sugimura, T. (1980) *Mutat. Res. 78*, 331−339.
10. Gueiffier, A., Chavignon, O., Navel, S., Chezal, J. M., Teulade, J. C., Blache, Y., and Chapat, J. P. (1996) *Heterocycl. Commun. 2*, 241−246.
11. Gueiffier, A., Viols, H., Chapat, J. P., Chavignon, O., Teulade, J. C., and Dauphin, G. (1990) *J. Heterocycl. Chem. 27*, 421−425.
12. Debouzy, J. C., Gueiffier, A., Fauvelle, F., Lhassani, M., Kerbal, A., Peinnequin, A., Dejean, E., Neirinck, V., Bachelet, C., and Chapat, J. P. (1996) *Boll. Chim. Farm. 135*, 192−198.
13. Feigon, J., Denny, W. A., Leupin, W., and Kearns, D. R. (1984) *J. Med. Chem. 27*, 450−465.
14. Debouzy, J. C., Gueiffier, A., Fauvelle, F., Viols, H., Dejean, E., Neirinck, V., Peinnequin, A., Bachelet, C., Perly, B., and Chapat, J. P. (1996) *J. Pharm. Sci. 85*, 200−205.
15. Debouzy, J. C., Crouzy, S., Dabouis, V., Gueiffier, A., Brasme, B., Bachelet, C., Favier, A., Simorre, J. P., Mazet, L., and Peinnequin, A. (1999) *Arch. Biochem. Biophys. 367*, 202−215.
16. Dabouis, V., Debouzy, J. C., Gueiffier, A., and Crouzy S. (1999) *Boll. Chim. Farm. 138*, 453−460.
17. Marion, D., and Wüthrich, K. (1983) *Biochem. Biophys. Res. Commun. 113*, 967−974.
18. Rance, M., Sorensen, O. W., Bodenhausen, G., Wagner, G., Ernst, R. R., and Wüthrich, K. (1983) *Biochem. Biophys. Res. Commun. 117*, 479−485.
19. Braunschweiler, L., and Ernst, R. R. (1983) *J. Magn. Reson. 53*, 521−528.
20. Bax, A., and Davis, D. G. (1985) *J. Magn. Reson. 63*, 207−213.
21. Bax, A., and Davis, D. G. (1985) *J. Magn. Reson. 65*, 355−360.
22. States, D. J., Haberkorn, R. A., and Ruben, D. J. (1982) *J. Magn. Reson. 48*, 286−292.
23. Macura S., and Ernst R. R. (1980) *Mol. Phys. 41*, 95.
24. Piotto, M., Saudek, V., and Sklenar, V. (1992) *J. Biomol. NMR 2*, 661−665.

25. Wüthrich, K. (1986) in *NMR of proteins and nucleic acids*, Wiley, New York.
26. Plavec, J., and Chattopadyana, J. (1995) *Tetrahedron Lett. 36*, 1949−1952.
27. Lankhorst, P. P., Haasnoot, C. A., Erkelens, C., and Altona, C. (1984) *J. Biomol. Struct. Dyn. 1*, 1387−1405.
28. Clore, G. M., Nilges, M., Brunge, A., and Gronenborn, A. M. (1988) *Eur. J. Biochem. 171*, 479−484.
29. Clore, G. M., Murphy, E. C., Gronenborn, A. M., and Bax, A. (1998) *J. Magn. Reson. 134*, 164−167.
30. Clore, G. M., Brünger, A. T., Karplus, M., and Gronenborn, A. M. (1986) *J. Mol. Biol. 191*, 523.
31. Nilges, M., Clore, G. M., and Gronenborn, A. M. (1988) *FEBS Lett. 239*, 129−136.
32. Brünger, A. T., and Karplus, M. (1990) *Acc. Chem. Res. 24*, 54−61.
33. Nilges, M., Clore, G. M., and Gronenborn, A. M. (1988) *FEBS Lett. 229*, 317−324.
34. Nilges, M., Gronenborn, A. M., Brünger, A. T., and Clore G. M. (1988) *Protein Eng. 2*, 27−38.
35. Blackledge, M. J., Medvedeva, S., Poncin, M., Guerlesquin, F., Bruschi, M., and Marion, D. (1995) *J. Mol. Biol. 245*, 661−681.
36. Brooks, B. R., Broccoleri, R. E., Olafson, B. D., States, D. J., Swaminarthan, S., and Karplus, M. J. (1983) *J. Comput. Chem. 4*, 187−217.
37. Weiner, S. J., Kollman, P. A., Case, D. A., Singh, U. C., Ghio, C., Alagona, G., Profeta, S., and Weiner, P. (1984) *J. Am. Chem. Soc. 106*, 765−784.
38. Schmidt, W., Baldridge, K. K., Boatz, J. A., Elbert, S. T., Gordon, M. S., Jensen, J. J., Koseki, S., Matsunaga, N., Nguyen, K. A., Su, S. W. T. L., Dupuis, M., and Montgomery, J. A. (1993) *Comput. Chem.*, 1347−1363.
39. MacKerell, A. D. J. (1998) *J. Phys. Chem. 102*, 3586−3616.
40. Waltham, M. A. (1993) in *Molecular Simulations*.
41. Van-Gunsteren, W. F., and Berendsen, H. J. C. (1977) *Mol. Phys. 34*, 1311−1327.
42. Kaplan, J. I., and Fraenkel, G. (1980) in *NMR of chemically exchanging systems*, Academic Press Inc., New York.
43. Feigon, J., Denny, W. A., Leupin, W., and Kearns, D. R. (1984) *J. Med. Chem. 27*, 450−465.
44. Job, P. (1928) *Ann. Chim. 9*, 113−125.
45. Gorenstein, D. G. (1984) in *^{31}P NMR: principles and applications*, Pergamon Press, New York.
46. Marion, D., and Lancelot, G. (1984) *Biochem. Biophys. Res. Commun. 124*, 774−779.
47. Williams, H. E., and Searle, M. S. (1999) *J. Mol. Biol. 290*, 699−716.
48. Adams, A., Guss, J. M., Collyer, C. A., Denny, W. A., and Wakelin, L. P. (1999) *Biochemistry 38*, 9221−9233.
49. Debouzy, J. C., Gueiffier, A., and Dabouis, V. (1998) *Ann. Pharm. Fr. 56*, 197−204.
50. Delbarre, A., Delepierre, M., Garbay, C., Igolen, J., Le Peck, J. B., and Roques, P. (1987) *Proc. Natl. Acad. Sci. U.S.A. 84*, 2155−2159.
51. Hu, G. G., Shui, X., Leng, F., Priebe, W., Chaires, J. B., and Williams, L. D. (1997) *Biochemistry 36*, 5940−5946.
52. Moore, M. H., Hunter, W. N., d'Estaintot, B. L., and Kennard, O. (1989) *J. Mol. Biol. 206*, 693−705.
53. Gao, Y. G., and Wang, A. H. (1991) *Anti-cancer Drug Des. 6*, 137−139.
54. Berger, I., Su, L., Spitzner, J. R., Kang, C., Burke, T. G., and Rich, A. (1995) *Nucleic Acids Res. 23*, 4488−4494.

BI0024963